CHEMISTRY
A EUROPEAN JOURNAL

Fine-Tuning the Electronic Properties of Highly Stable Organometallic Cu^{III} Complexes Containing Monoanionic Macrocyclic Ligands

Raül Xifra,[a] Xavi Ribas,*[a] Antoni Llobet,*[b] Albert Poater,[c] Miquel Duran,[c] Miquel Solà,*[c] T. Daniel. P. Stack,[d] Jordi Benet-Buchholz,[e] Bruno Donnadieu,[f] José Mahía,[g] and Teodor Parella[h]

Abstract: A family of highly stable organometallic Cu^{III} complexes with monoanionic triazamacrocyclic ligands (L^i) with general formula $[CuL^i]^+$ have been prepared and isolated, and their structural, spectroscopic, and redox properties thoroughly investigated. The HL^i ligands have been designed in order to understand and quantify the electronic effects exerted by electron donor and electron-withdrawing groups on either the aromatic ring or the central secondary amine or on both. In the solid state the Cu^{III} complexes were mainly characterized by single-crystal X-ray diffraction analysis, whereas in solution their structural characterization was mainly based on ^1H NMR spectroscopy given the diamagnetic nature of the d^8 square-planar Cu^{III} complexes. Cyclic voltammetry together with ^1H NMR and UV/Vis spectroscopy have allowed us to quantify the electronic effects exerted by the ligands on the Cu^{III} metal center. A theoretical analysis of this family of Cu^{III} complexes has also been undertaken by DFT calculations to gain a deeper insight into the electronic structure of these complexes, which has in turn allowed a greater understanding of the nature of the UV/Vis transitions as well as the molecular orbitals involved.

Keywords: C–H activation · copper(III) complexes · density functional calculations · electrochemistry · spectroscopic properties

Introduction

The controlled activation of small and relatively inert molecules by transition-metal complexes (TMC) under mild conditions is a very active area of research that has made impressive advances over the last 20 years.[1] In particular, the activation of C–H bonds in saturated hydrocarbons is of special interest since these are the major constituents of natural gas and petroleum.[2] However, the full potential of TMC in profitable practical applications, for example, in catalytic conversion to more valuable products, has not yet been realized.[3]

By choosing the appropriate ligands and metal, a remarkable degree of control over the activation processes can be

[a] Dr. R. Xifra, Dr. X. Ribas
Departament de Química, Universitat de Girona
Campus de Montilivi, 17071, Girona (Spain)
E-mail: xavi.ribas@udg.es

[b] Prof. A. Llobet
Departament de Química, Universitat Autònoma de Barcelona
Bellaterra, 08193 Barcelona (Spain)
Fax: (+34) 935-813-101
E-mail: antoni.llobet@uab.es

[c] A. Poater, Prof. M. Duran, Prof. M. Solà
Institut de Química Computacional, Universitat de Girona
Campus de Montilivi, 17071, Girona (Spain)
Fax: (+34) 972-418-356
E-mail: miquel.sola@udg.es

[d] Prof. T. D. P. Stack
Department of Chemistry, Stanford University
Stanford, CA 94305–5080 (USA)

[e] Dr. J. Benet-Buchholz
Institut Català d'Investigació Química (ICIQ)
Avgda. Països Catalans, s/n, 43007 Tarragona (Spain)

[f] Dr. B. Donnadieu
Service de Cristallochimie, Laboratoire de Chimie de Coordination
UPR CNRS 8241, Route de Narbonne 205, 31077, Toulouse Cedex 4 (France)

[g] Dr. J. Mahía
Servicios Xerais de Apoio Á Investigación
Universidade da Coruña, 15071 A Coruña (Spain)

[h] Dr. T. Parella
Servei de RMN, Universitat Autònoma de Barcelona
Bellaterra, 08193 Barcelona (Spain)

Supporting information for this article is available on the WWW under http://www.chemeurj.org/ or from the author.

DOI: 10.1002/chem.200500088

accomplished under mild conditions, which in turn can lead to the improved efficiency and selectivity of the whole process.[4]

In a recent paper we presented a novel aryl C–H activation process involving Cu^{II} complexes that leads to the formation of relatively unusual and stable Cu^{III} complexes containing a monoanionic ligand.[5]

Few d^8 Cu^{III} complexes have been structurally characterized by single-crystal X-ray diffraction and those that have all exhibit a square-planar type of geometry. The higher oxidation state is stabilized either by the presence of a trianionic ligand derived from the deprotonation of tripeptides,[6] corroles[7] or confused porphyrins,[8] or by the participation of several ligands supplying overall at least three negative charges, such as the trifluoromethanate ligand.[9] The different factors that govern Cu^{III} stabilization and its reactivity are of considerable interest in biology since Cu^{III} is the active center of certain metalloproteins[10] and also because Cu^{III} is thought to be responsible for the oxidative degradation and site-specific cleavage of DNA.[11] Furthermore Cu^{III} has been postulated as an intermediate in the oxidation of saturated hydrocarbons using copper complexes as oxygen and/or hydrogen peroxide activators, a variation of the so-called Gif chemistry developed by Barton et al.[12]

Herein we present the synthesis and characterization of a family of $[Cu^{III}L^i]^{2+}$ macrocyclic complexes, generated via C–H activation using the corresponding $[Cu^{II}(HL^i)]^{2+}$ complexes, containing the ligands displayed in Scheme 1. These ligands have been chosen to enable us to gain some understanding of the influence of steric and electronic effects on the properties of the Cu^{III} complexes.

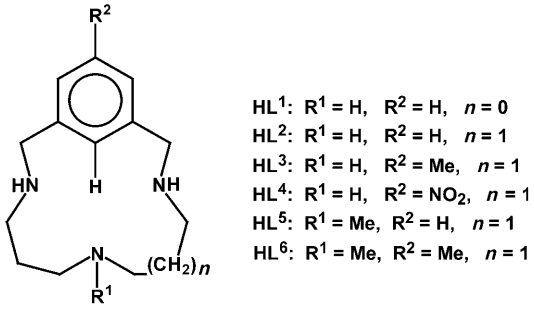

Scheme 1. Triazamacrocyclic ligands HL^i ($i=1$–6).

Results and Discussion

Synthesis and X-ray structures: The triazamacrocyclic ligands used in this work are depicted in Scheme 1. In general, these ligands were prepared by the cyclization of the corresponding 1,3-bis(bromomethyl)benzene with the appropriate tosylated triamine following a similar methodology (see Scheme 2 for the particular case of HL^3) to that first described by Bencini et al.[13] for related compounds. The tosylated triazamacrocycles were then treated with lithium suspended in liquid ammonia[14] to afford the triazamacrocyclic ligands HL^i in moderate-to-good yields. The ligands HL^3, HL^4, and HL^6, which contain Me- and NO_2-substituted aryl groups, are described and characterized for the first time in this work, whereas the other three have been reported previously.[5,15] The detosylation process can also be carried out with HBr/HAcO/phenol to give the same organic compounds but with better yields.[13] The new HL^i ligands have been thoroughly characterized by the usual analytical and spectroscopic techniques and the data are presented in the Supporting Information.

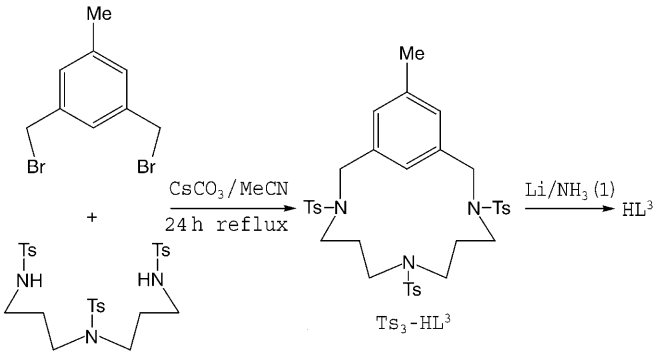

Scheme 2. Synthetic strategy for the preparation of the triazamacrocyclic ligand HL^3.

Under anaerobic conditions at room temperature, the HL^i ligands react instantaneously with Cu^{II} salts (triflate or perchlorate) in acetonitrile to afford the corresponding unstable $[Cu^{II}(HL^i)]^{2+}$ complexes, which quantitatively disproportionate to generate a colorless Cu^{I} and an orange Cu^{III} complex [Eq. (1)], both of which are diamagnetic.

$$2[Cu^{II}(HL^i)]^{2+} \overset{MeCN,\ RT}{\rightleftharpoons} [Cu^{III}(L^i)]^{2+} + [Cu^{I}(H_2L^i)]^{2+} \quad (1)$$

Diffusion of diethyl ether into the resulting acetonitrile solution overnight results in the precipitation of red microcrystals of $[Cu^{III}(L^i)]^{2+}$ (**1**–**6**, $i=1$–6) in nearly quantitative yield. These six Cu^{III} complexes, **1**–**6**, are all stable in the solid state and in both protic (H_2O, pH 1–7; MeOH) and aprotic solvents (MeCN, CH_2Cl_2) under aerobic conditions except for **4** which decomposes in solution at room temperature as a result of the strong electron-withdrawing nature of the nitro substituent. Under basic conditions the Cu^{III} complexes readily transform into the corresponding dinuclear diphenoxo complexes of general formula $[Cu^{II}_2(\mu\text{-}OL^i)_2]^{2+}$, which will be reported elsewhere.

^{1}H NMR spectroscopic analysis of the reaction mixture, performed by using CD_3CN as the solvent, allowed us to confirm that the reaction proceeded by disproportionation by simple integration of the Cu^{I} and Cu^{III} resonances. Furthermore, optical titration of the reaction mixture with excess phenanthroline also confirms a 50% conversion of Cu^{II} to Cu^{I}.

Complex **2** reacts with Cl^- at room temperature to form a pentacoordinate copper complex, $[Cu^{III}(L^2)Cl]^+$, **7**, whose structure will be discussed below. In a similar manner, **4**, which contains the NO_2 electron-withdrawing group, also reacts readily with Cl^- stabilizing the resulting nitro com-

plex $[Cu^{III}(L^4)Cl]^+$, **8**, although its isolation in the solid state still remains elusive as a result of decomposition.

Crystallographic data and selected bond lengths and angles for complexes **2**, **3**, **6** and **7** are reported in Table 1 and Table 2, respectively. ORTEP views of these complexes together with their labeling schemes are shown in Figure 1 and in the Supporting Information. In complexes **1**, **2**, **3**, **5**, and **6**, the Cu^{III} metal center is coordinated to the three nitrogen atoms of the macrocyclic ligand and a carbon atom of the phenyl ring and adopts a distorted square-planar geometry. The shortest coordination distance is always the organometallic Cu1–C1 bond, which ranges from 1.848 Å for **1** to 1.926 Å for **6**. This is in agreement with the fact that the macrocyclic ligand, L^1, of complex **1** has the smallest cavity of this series and also with the fact that the longest Cu1–C1 distance is that of complex **6**, which contains a ligand, L^6, with a tertiary amine. The *trans* effect produced by the Cu1–C1 bond generates the longest Cu–N distances (Cu1–N2 bond lengths range from 1.995 Å for **3** to 2.048 Å for **6**) and are 0.033–0.095 Å longer than the mean distances of the other two Cu–N bonds (Cu1–N1 and Cu1–N3). This is especially acute for complexes **5** and **6** which contain the macrocyclic ligands L^5 and L^6 with the methylated central amine. This phenomenon has been described in detail previously mainly by Meyerstein and co-workers[16] and by Bernhardt;[17] the M–N bond strength of tertiary amines is weaker than that of secondary amines under comparable conditions. Herein this phenomenon will from now on be termed the "*N*-methylation effect". The increase in the steric crowding and strain around the tertiary nitrogen atom of the amine together with solvation effects through hydrogen bonding are identified as the main factors that produce this effect.[18]

The *N*-methylation effect of the tertiary amines, besides the elongation of the $Cu–N_{tert}$ bond, is also structurally manifested in our case through a geometrical distortion. This distortion involves the torsion angles between the best-fitted plane that contains the carbon framework of the aromatic ring and the best-fitted plane that contains the C1, Cu1, N1, and N3 atoms (the first coordination sphere of the copper center with the exception of the nitrogen atom of the tertiary amine). In complexes **5** and **6**, which contain a tertiary amine, this torsion angle is 9.4 and 9.6°, respectively, whereas in complexes **2** and **3** this distortion is reduced to 7.4 and 2.1°, respectively, thus showing a lower degree of distortion (the mathematical equations describing the best-fitted planes as well as the distances of all the atoms to the planes are presented in the Supplementary Information).

Table 2. Selected bond lengths [Å] and angles [°] for complexes **1**–**3** and **5**–**7**.

	1[a]	**2**	**3**[b]	**5**[a]	**6**	**7**
C1–Cu1	1.848(4)	1.901(2)	1.902(2)	1.905(3)	1.926(8)	1.898(6)
N1–Cu1	1.899(4)	1.960(2)	1.961(2)	1.985(3)	1.957(7)	1.958(5)
N3–Cu1	1.911(3)	1.952(2)	1.963(2)	1.961(3)	1.963(7)	1.963(5)
N2–Cu1	2.000(8)	2.002(2)	1.995(2)	2.031(3)	2.048(7)	1.988(5)
C1-Cu1-N1	84.600(2)	82.800(1)	82.000(1)	82.900(2)	84.100(3)	82.200(2)
C1-Cu1-N3	84.400(2)	81.700(1)	82.200(1)	82.300(2)	82.600(4)	81.100(2)
N1-Cu1-N2	105.600(2)	95.600(1)	97.400(1)	96.900(1)	94.300(3)	94.700(2)
N2-Cu1-N3	85.200(2)	99.700(1)	96.400(1)	99.700(1)	97.600(3)	99.300(2)
C1-Cu1-N2	163.500(2)	178.400(1)	173.800(1)	177.600(1)	173.800(3)	171.900(2)
N1-Cu1-N3	169.000(2)	157.200(1)	156.000(1)	160.700(2)	161.000(4)	154.500(2)
Cu–O (short)	2.428(3)	2.408(2)	2.256(2)	2.442(4)	2.279(5)	2.556(2) (Cl)[c]
Cu–O (long)	2.584(3)	2.643(2)	2.835(2)	2.736(4)	3.662(5)	3.301(2) (Cl)[c]
O-Cu-O	170.9(2)	156.6(1)	161.0(1)	177.3(1)	148.01(3)	160.7(2) (Cl)[c]

[a] See reference [5]. [b] There are two different molecules in the unit cell with very similar metric parameters. [c] The values shown here for complex **7** are the shortest Cu–Cl distances and the smallest Cl–Cu–Cl angles (see Figure 2 for the other values).

Table 1. Crystal data and structure refinement of Cu^{III} complexes.

	2-$(OTf)_2$	**3**-$(OTf)_2$	**6**-$(OTf)_2$	**7**-(ClO_4)
empirical formula	$C_{16}H_{22}Cu_1F_6N_3O_6S_2$	$C_{17}H_{24}Cu_1F_6N_3O_6S_2$	$C_{18}H_{26}Cu_1F_6N_3O_6S_2$	$C_{28}H_{44}Cu_2N_6O_8Cl_4$
M_r	594.03	608.05	622.08	861.70
crystal system	monoclinic	monoclinic	monoclinic	orthorhombic
space group	*P*21/*c*	*P*21/*c*	*P*21/*c*	*Pbca*
a [Å]	9.603(2)	24.727(1)	24.163(5)	16.959(1)
b [Å]	8.777(2)	12.4908(3)	14.822(3)	18.088(2)
c [Å]	26.476(5)	15.8686(4)	17.658(4)	22.441(1)
α [°]	90	90	90	90
β [°]	98.08(3)	107.265(1)	127.83(3)	90
γ [°]	90	90	90	90
V [Å^3]	2209.4(8)	4680.3(2)	4995.0(2)	6884.0(8)
Z	4	8	8	8
temperature [K]	160(2)	153(2)	180(2)	160(2)
$\lambda(Mo_{K\alpha})$ [Å]	0.71073	0.71073	0.71073	0.71073
ρ_{calcd} [g cm^{-3}]	1.786	1.726	1.670	1.663
μ [mm^{-1}]	1.268	1.199	1.129	1.604
R[a]	0.0295	0.0409	0.0730	0.0548
R_w[b]	0.0765	0.1026	0.1569	0.0895

[a] $R=\Sigma[F_0-F_C]/\Sigma F_0$. [b] $R_w=\{\Sigma[w(F_0^2-F_c^2)^2]/\Sigma(wF_0^4)\}^{1/2}$.

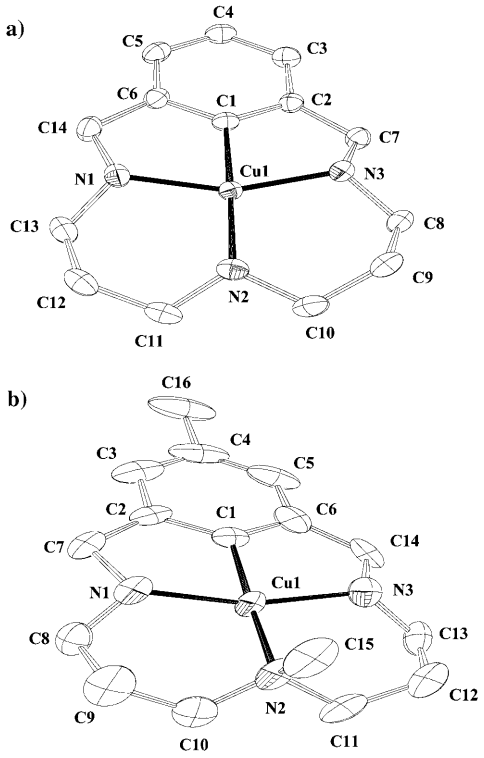

Figure 1. ORTEP plot (50% probability) of the cationic moiety of the X-ray crystal structures of complexes a) **2** and b) **6**. Hydrogen atoms have been omitted for clarity.

Note also that in all cases the hydrogen atoms bonded to the secondary amines (**2** and **3**) are oriented in the same direction and thus the macrocyclic ligand adopts a *syn* conformation. This *syn* conformation is also adopted by macrocyclic ligands with methylated central amines (**5** and **6**). The non-anionic nature of the nitrogen-coordinating atoms is in line with the longest Cu^{III}–N bonds found in this family of complexes relative to the bond lengths found in other Cu^{III} complexes that contain deprotonated amides as ligands.[6,19]

In complexes **1**–**3**, **5**, and **6** the ClO_4^- or $CF_3SO_3^-$ counteranions or a water molecule (in the case of complex **6**) are weakly associated with the metal center, generating a decompressed tetragonally distorted octahedral environment in which one of the Cu–O distances is substantially longer than the other (see Table 2). In all cases, the longer Cu–O distance is located on the same side of the macrocycle as the N–H or N–Me bonds, whereas the shorter Cu–O distance is located on the other side which has a much lower steric encumbrance. This distorted octahedral environment is perhaps the most salient feature of this family of compounds[5] in comparison with Cu^{III} complexes described previously[6–9] and can be attributed to the fact that in our case the higher oxidation state of the copper center is stabilized by a monoanionic ligand.

In complex **7**, the Cu^{III} metal center adopts a similar geometry as in the previous cases except that the axial positions are occupied by chlorine instead of oxygen atoms, which at the same time bridge two metal centers. Furthermore, this complex exhibits two crystallographically distinct molecules in its unit cell (their atoms are thus labeled by adding the letters "a" or "b", for example, the copper atoms are labeled Cu1a and Cu1b), although their parameters are very similar. While the crystal packing in the complexes **1**–**6** is unremarkable, the chlorine bridge in **7** produces pseudochains along the *z* axis with alternating "a" and "b" molecules, as shown in Figure 2.

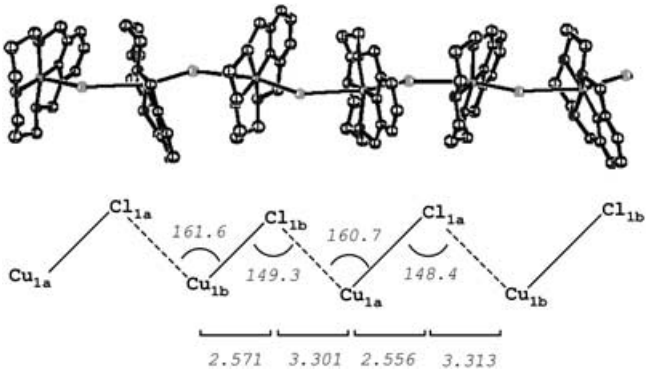

Figure 2. Crystal packing for complex **7** showing the formation of a pseudochain through the Cu–Cl bonds; structural parameters are also indicated.

Spectroscopic properties: The 1D and 2D NMR spectra of the Cu^{III} complexes **1**–**8** and their corresponding ligands HL^1–HL^6 were recorded in CD_3CN and are presented in the Supporting Information. The combination of 1D and 2D NMR spectra has allowed us to unambiguously identify the resonances of all the protons in the complexes and ligands. Their assignments are reported in the Experimental Section and in Table 3 and are consistent with the structures found in the solid state.

Table 3 also contains the coordination-induced shifts (CIS) as well as the Methylation-induced shifts (MeIS). The latter is defined as the difference in chemical shift for a particular resonance when the central amine is methylated and when it is not and thus remains a secondary amine. This shift has been introduced here to analyze the electronic effects produced by methylation.

A careful examination of the data in Table 3 reveals the following trends. 1) In both the ligands and complexes, the Me and NO_2 substituents in the aromatic ring significantly affect the δ values of the remaining aromatic protons, very slightly affect the benzylic resonances, and virtually have no affect on the aliphatic resonances. 2) In all cases, with the exception of the aromatic protons, complexation produces a positive CIS, the highest values being observed for the benzylic and aminic methyl groups (0.6–0.7 ppm). The negative CIS values observed for the aromatic protons suggest that the aromatic rings, besides acting as σ donors, also act as weak π acceptors. 3) In the ligands, a negative MeIS is observed for all the methylenic protons (H_{b-d}) neighboring the

Table 3. Chemical shifts, CIS, and MeIS for the ligands HL^2–HL^6 and complexes **2**–**6**.[a]

	HL^2	HL^3	HL^4	HL^5	MeIS[b]	HL^6	MeIS[b]	**2**-$(ClO_4)_2$	CIS[c]	**3**-$(OTf)_2$	CIS[c]	**4**-$(OTf)_2$	CIS[c]	**5**-$(ClO_4)_2$	CIS[c]	MeIS[b]	**6**-$(OTf)_2$	CIS[c]	MeIS[b]
H_y	7.25	–	–	7.24		–		7.27	0.02	–		–		7.27	0.03	0.00	–		
H_z	7.11	6.91	7.95	7.07		6.88		6.95	−0.16	6.78	−0.13	7.9	−0.05	6.95	−0.12	0.00	6.77	−0.11	−0.01
H_α	[d]	[d]	[d]	[d]		[d]		6.12		6.96		[d]		6.33			7.11		
H_β	[d]	[d]	[d]	[d]		[d]		3.14		3.77		[d]		–			–		
H_{a1}	3.87	3.84	3.98	3.9	0.03	3.84	0.00	4.61	0.68	4.65	0.70	4.75	0.67	4.67	0.70	0.05	4.67	0.76	0.06
H_{a2}								4.49		4.42		4.55		4.52			4.52		
H_{b1}	2.84	2.78	2.77	2.5	−0.34	2.5	−0.26	3.09	0.02	3.27	0.43	2.64	−0.01	3.05	0.36	0.00	3.37	0.76	0.05
H_{b2}								2.63		3.15				2.67			3.15		
H_{c1}	1.68	1.66	1.65	1.63	−0.05	1.61	−0.05	1.77	0.23	2.10	0.38	1.96	0.31	2.15	0.42	0.15	2.33	0.57	0.14
H_{c2}	–							2.04		1.98				1.95			2.02		
H_{d1}	2.56	2.52	2.53	2.49	−0.07	2.46	−0.06	2.99	0.53	2.90	0.48	2.97	0.52	3.08	0.67	0.08	3.21	0.49	−0.06
H_{d2}	–							3.18		3.10		3.12		3.24			2.68		
H_e	–	–	–	2.01		2		–		–		–		2.73	0.72		2.91	0.91	
H_f	–	2.34	–	–		2.30		–		2.31	−0.03	–		–			2.28	−0.02	−0.03

[a] See Scheme 1 for labels. [b] The methylation induced shift (MeIS) is defined as the difference between the chemical shift of a particular proton in a methylated compound and the same proton in the corresponding non-methylated compound. For CH_2 methylenic groups with magnetically different protons the MeIS is calculated by taking the mean value. [c] In the CIS of the complexes, the mean value of the chemical shifts of two magnetically different protons of each CH_2 methylenic group is subtracted from the chemical shift displayed by the same protons in the free ligand. [d] Not observed.

central amine as a consequence of the electron-donating effect exerted by the methyl group (see Scheme 3 for the atomic labeling used in the NMR assignment). The H_d protons, in the α position, are as expected the ones that are most affected. 4) In sharp contrast, the opposite effect is observed in the complexes with positive MeIS values for the H_{b-d} protons. Furthermore, the most affected proton is now H_c, which is in a β position with respect to the central amine, followed by H_d, and finally H_b is only slightly affected.

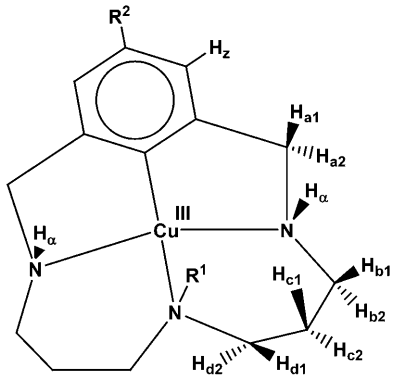

	R^1	R^2
2	H_β	H_y
3	H_β	$C(H_f)_3$
4	H_β	NO_2
5	$C(H_e)_3$	H_y
6	$C(H_e)_3$	$C(H_f)_3$

Scheme 3. Drawings and ^1H NMR labeling scheme for the cationic moiety of Cu^{III} complexes **2**–**6**.

This inversion of the MeIS for the complexes reveals that from an electronic point of view the methyl group situated at the tertiary amine paradoxically acts as an electron-withdrawing group. This is further supported by the $E_{1/2}$ redox potentials of the Cu^{III}/Cu^{II} couple bearing the methylated tertiary amines since they are anodically shifted relative to those of the non-methylated secondary amine (vide infra). This effect has previously been observed in aqueous solutions of non-organometallic Cu^{II} complexes[16,17] and was attributed to a number of factors including the formation of hydrogen bonds between the secondary amines and solvent molecules and less metal–ligand orbital overlap as a result of the steric effects generated by the methylated tertiary amine which displace the nitrogen bonding electron pair out of the main plane in which the metal center is located. Indeed, the latter effect can also be observed in the complexes described in this paper since the methylated complexes **5** and **6** have the highest angles between the planes defined by the carbon atoms of the aromatic ring and the C1, Cu1, N1, and N3 atoms (vide supra).

The UV/Vis spectra of complexes **2**–**7** are presented in Figure 3 and their λ_{max} values together with the corresponding extinction coefficients are listed in Table 4. The complexes **2**–**7** display a very intense band below 300 nm and another less intense but broad band in the range of 370–520 nm (see Figure 3) that can be assigned to two similar $\pi \rightarrow d_{x^2-y^2}$ ligand-to-metal charge transfer (LMCT) transitions.[20] As shown in Table 4 and Figure 3 (see also the de-

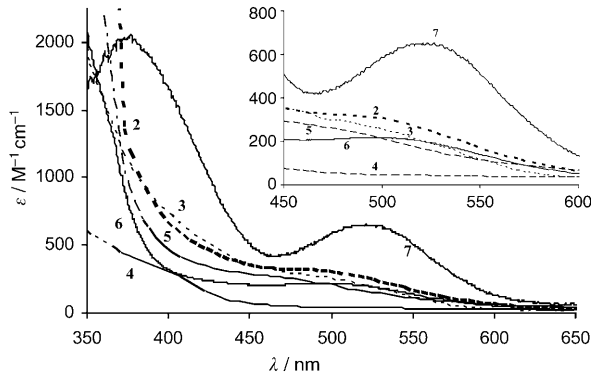

Figure 3. UV/Vis spectra for complexes **2**–**7**. The inset shows an enlargement of the 450–600 nm zone (see text for experimental details).

Table 4. Calculated and experimental deconvoluted UV/Vis data assigned to $\pi_1 \rightarrow d_{x^2-y^2}$ and $\pi_2 \rightarrow d_{x^2-y^2}$ transitions.

Complex	$\pi_1 \rightarrow d_{x^2-y^2}$		$\pi_2 \rightarrow d_{x^2-y^2}$	
	λ_{max}(exp.[a]) [nm]	λ_{max}(theor.) [nm]	λ_{max}(exp.[a]) [nm]	λ_{max}(theor.) [nm]
2	390(417)	552	463(147)	608
3[b]	487(303)	649	388(559)	617
4	277(325)	496	380(15)	567
5	393(345)	560	478(157)	623
6[b]	503(198)	661	397(285)	634
7	328(630)	469	386(1260)	497

[a] Extinction coefficients are given in parentheses and are measured in $M^{-1}cm^{-1}$. [b] The energies of the π_1 and π_2 orbitals are inverted compared with the energies of the other complexes; see text, Figure 5 and the Supporting Information for details.

convoluted spectra presented in the Supporting Information), the $\pi_1 \rightarrow d_{x^2-y^2}$ band for complexes **3, 5**, and **6** is red-shifted relative to **2**, while for complexes **4** and **7** a blue shift is observed.

Density functional theory (DFT) calculations (see Computational Details in the Experimental Section) were carried out for complexes **2**–**7** to elucidate the electronic properties of these complexes and thus understand the nature of the transitions observed in the UV/Vis spectra. For complex **2**, the DFT-optimized structure nicely fits the experimental X-ray structure (see the calculated structure and the comparison of the geometrical parameters presented in the Supporting Information) thus validating the adequacy of the theoretical method employed for the geometry optimizations of these particular systems.

Time-dependent DFT calculations (TDDFT) show that the most intense band below 300 nm involves the LUMO frontier orbital (Figure 4a) as the main arrival orbital for complex **2** (only small differences are observed for complexes **2**–**7**) and the σ_1 orbital (Figure 4b) as the main starting one. The LUMO orbital is mainly a combination of the $d_{x^2-y^2}$ orbital of the copper atom and the p orbitals of the nitrogen atoms and the carbon atom that participates in the Cu–C bond. In **7** there is an extra contribution from the p_z orbital of the chlorine atom.

The σ_1 orbital depicted in Figure 4b is composed essentially of the p_y orbitals of the atoms contained in the axis N2–Cu1–C1. This orbital is the HOMO-2 except in complex **4**, in which it is the HOMO-3 owing to the insertion of an orbital with mainly nitro-group character as the HOMO-2 orbital, and in complex **7**, in which the σ_1 orbital is the HOMO-6 because of the intercalation of three orbitals with Cu–Cl antibonding character and another orbital of macrocyclic character related to the Cu–N bonding interaction.

The $\pi \rightarrow d_{x^2-y^2}$ LMCT band is composed of two charge-transfer excitations, principally from the ligand to the metal. The main arrival orbital is the LUMO (see Figure 4a), but the starting orbital changes depending on the system. The first excitation starts from the π_1 orbital (Figure 4c), while the second one starts from the π_2 orbital (Figure 4d). The π_1 and π_2 orbitals are the HOMO and HOMO-1 orbitals in complexes **2**, **4**, and **5**. In the other complexes, these two orbitals are exchanged, except in complex **7** in which the π_1 and π_2 orbitals are the HOMO-3 and HOMO-4, respectively. The solvent has a significant effect on the energy of the $\pi \rightarrow d_{x^2-y^2}$ LMCT band and a less strong one on the band below 300 nm. After including this effect in the calculations, the $\pi \rightarrow d_{x^2-y^2}$ LMCT bands are blue-shifted, this shift being more noticeable in solvents with high dielectric constants.

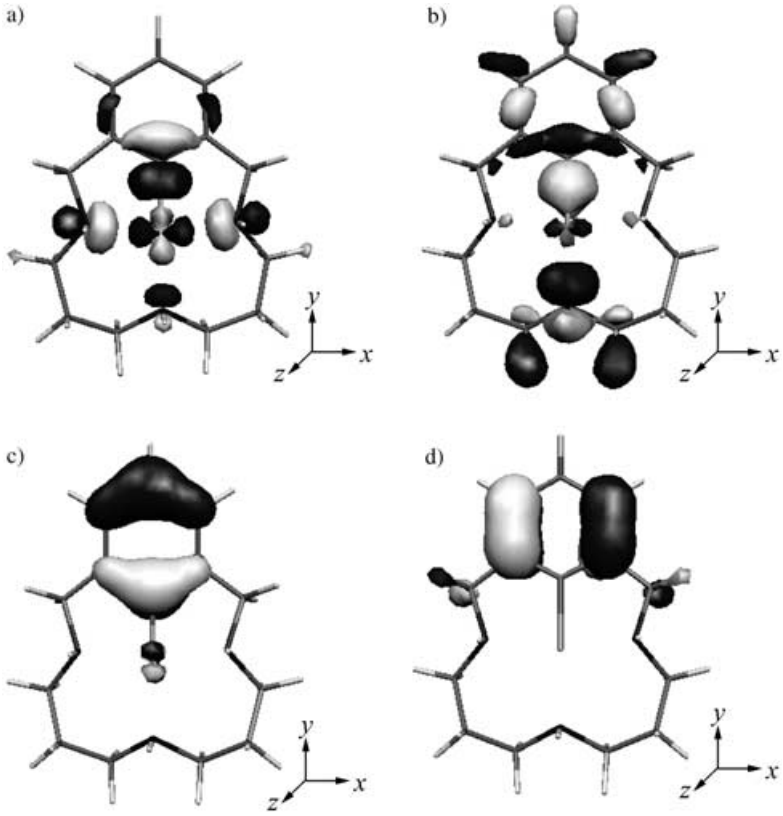

Figure 4. 3D representation of the orbitals most involved in the calculated excitations of the UV/Vis spectra of complex **2**: a) the LUMO orbital; b) the starting orbital (σ_1) involved in the highest energy band; c) the starting orbital (π_1) involved in the $\pi_1 \rightarrow d_{x^2-y^2}$ excitation; d) the starting orbital (π_2) involved in the $\pi_2 \rightarrow d_{x^2-y^2}$ excitation. Isosurface values are −0.05 and 0.05 a.u.

Figure 5 shows the energies of the orbitals and the wavelengths of the two calculated excitations that produce the

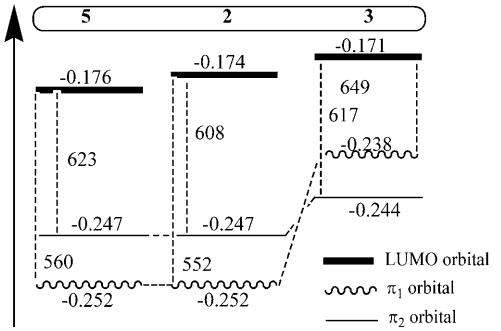

Figure 5. Calculated qualitative energy diagram of the orbitals involved in the π–$d_{x^2-y^2}$ LMCT bands of complexes **2**, **3**, and **5**. The orbital energies are given in atomic units (hartrees) and the wavelengths of the excitations in nm.

$\pi \rightarrow d_{x^2-y^2}$ LMCT bands for complexes **2**, **3**, and **5**, whereas Table 4 and Figure S12 (Supporting Information) reveal the main features of the experimental and calculated LMCT transitions of complexes **2**–**7**. As can be observed from the data in Table 4, the experimental $\pi_1 \rightarrow d_{x^2-y^2}$ transition correlates well with the TDDFT calculated one with a shift of 141–167 nm for complexes **2**, **3**, **6**, and **7** and of 219 nm for **4**. Although the absorption wavelengths calculated by TDDFT are clearly overestimated, the errors are comparable to those found in similar studies.[21] These errors may be attributed to the size of the basis set,[22] the inadequate description of solvent effects, which are very relevant in charged species, and the different localized or delocalized character of the initial and final electronic states.[21a] However, we want to emphasize that our main goals are to tentatively assign the observed transitions and to understand the origin of the shifts experienced by the different bands when going from complex **2** to complexes **3**–**7**. In our opinion, these shifts are well reproduced by our calculations and an understanding of the origin of the shifts is provided by the analysis of the molecular orbitals that are most involved in the electronic transitions. Finally, the $\pi_2 \rightarrow d_{x^2-y^2}$ transition has a similar degree of correlation to that of the $\pi_1 \rightarrow d_{x^2-y^2}$ transition, with the exception of **3** and **6**, which are shifted in opposite directions.

Methylation of the aromatic ring of species **2** to yield complex **3** has a greater effect on the $\pi_1 \rightarrow d_{x^2-y^2}$ LMCT band than the methylation of the central amine in complex **5**. In both cases, the band is red-shifted, but the magnitude of the shift in the former is much larger (exptl: 97 nm, calcd: 97 nm for **3**; exptl: 3 nm, calcd 8 nm for **5**). Methylation in both places (complex **6**) causes a red shift that is nearly the sum of the two shifts described above (exptl: 113 nm, calcd: 109 nm for **6**).

By using complex **2** as a reference, it is found that the energies of the π_1 and π_2 orbitals remain almost constant after the methylation of the amine (complex **5**), while the LUMO is slightly stabilized, as expected from the fact that the methyl group behaves as an electron-acceptor group (vide supra) in this particular species (see Figure 5). Methylation of the aromatic ring in complex **3** has the opposite effect on the LUMO, that is, the LUMO is slightly destabilized, which is not surprising if one considers that this methyl group behaves as an electron donor. In line with this, the π_1 and π_2 orbitals in complex **3** are significantly destabilized owing to their proximity to the aromatic group. In fact, the π_1 orbital is destabilized more than the π_2 orbital because the methyl group bonded to the aromatic carbon contributes to the π_1 orbital with an antibonding interaction whereas it does not participate in the π_2 orbital. This effect is responsible for the relative inversion of the energies of the π_1 and π_2 orbitals in complexes **3** and **6** in which the methyl substituent is bonded to the phenyl group.

The significant destabilization of the π_1 and π_2 orbitals in complex **3** account for the larger red shift observed for complex **3** than for complex **5**.

The presence of a nitro group (complex **4**) in the aromatic ring causes a blue shift of the $\pi_1 \rightarrow d_{x^2-y^2}$ transition relative to complex **2** (exptl: 113 nm, calcd: 56 nm). This blue shift results from a greater stabilization of the π_1 and π_2 orbitals than of the LUMO giving a larger energy difference as a result of the electron-accepting nature of the nitro group.

In complex **7**, two bands were found experimentally at 375 and 522 nm. The band at 375 nm splits into two bands centered at 328 nm and 386 nm (Gaussian deconvolution). In this case, theoretical calculations were useful to understand and assign the origin of these transitions. It has been found that the band at 375 nm is a result of a $\pi \rightarrow d_{x^2-y^2}$ LMCT transition similar to that occurring in complexes **2**–**6** but the band at 522 nm arises from three transitions that start from antibonding σ^* and π^* orbitals of the Cu–Cl bond (HOMO, HOMO-1, and HOMO-2) (see Figure 6) and finish at the LUMO orbital.

Our calculations indicate that the $\pi_1 \rightarrow d_{x^2-y^2}$ LMCT transition in complex **7** is blue-shifted relative to the same transition in **2** (exptl: 62 nm, calcd: 83 nm). This blue shift results from the substantial destabilization of the LUMO orbital and at the same time an important stabilization of the π_1 and π_2 orbitals in this complex. The destabilization of the LUMO orbital is a result of the large charge transfer (0.62 *e*) from the chlorine anion to complex **2** that occurs in the formation of complex **7**.

Finally, our calculations also correctly predict much higher intensities for the $\pi \rightarrow d_{x^2-y^2}$ bands of the Cu–Cl complex **7** than for complexes **2**–**6** (see oscillator strength values in Table S5 and Figure S12 in the Supporting Information).

Redox properties: The redox properties of complexes **1**–**8** were investigated by means of cyclic voltammetric and coulometric techniques and their electrochemical parameters are given in Table 5. Figure 7 presents the cyclic voltammograms of complexes **2**–**6** and reveals a chemically and electrochemically quasireversible Cu^{III}/Cu^{II} redox couple. Coulometric experiments show that upon reduction to oxidation state II, the complexes described in this work are not stable, undergoing irreversible decomposition reactions. The Cu^{III}/Cu^{II} redox couple as expected depends on the electronic nature of the phenyl substituents as well as on the nature of

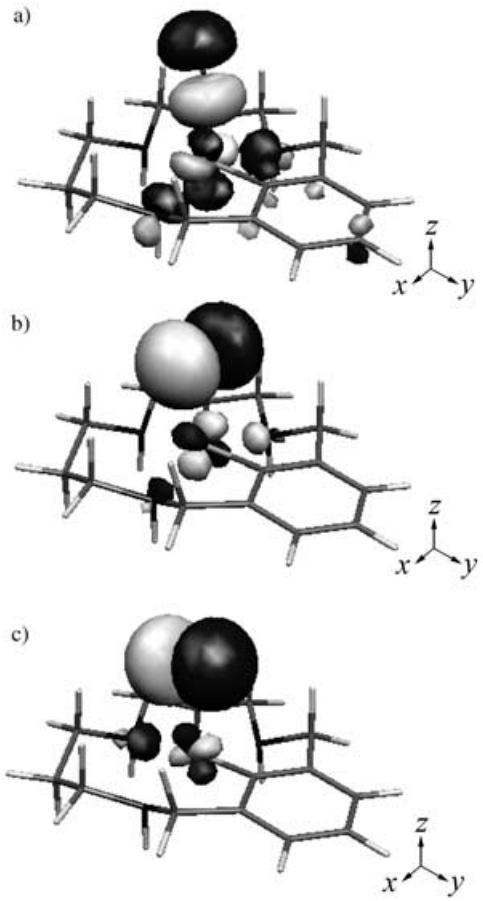

Figure 6. 3D representations of the starting orbitals most involved in the excitation at 522 nm in the experimental UV/Vis spectra of complex **7**: a) HOMO; b) HOMO-1; and c) HOMO-2 orbitals. Isosurface values are −0.05 and 0.05 a.u.

Table 5. Electrochemical parameters (versus SSCE) of complexes **1**–**8**.

Complex	$E_{1/2}$ [mV][a]	$E_{p,a}$ [V]	$E_{p,c}$ [V]	ΔE [mV]	$I_{p,a}/I_{p,c}$
1	–	–	−0.444	–	–
2	−163	−0.116	−0.210	94	0.9
3	−201	−0.152	−0.250	98	0.6
4	6	0.076	−0.063	139	0.9
5	−103	−0.056	−0.150	94	0.9
6	−129	−0.084	−0.174	90	0.8
7	–	–	−0.400	–	–
8	−271	−0.148	−0.394	246	1.0

[a] $E_{1/2}$ values referenced to the ferrocene/ferrocenium couple can be found in Table S6 of the Supporting Information.

the central macrocyclic amine. To evaluate these electronic effects, the Cu^{III}/Cu^{II} redox couple of complex **2** ($E_{1/2}=-0.163$ V; $E_{p,a}=-0.116$ V, $E_{p,c}=-0.210$ V, $\Delta E=94$ mV) was used as a reference. Electron-withdrawing substituents in the phenyl ring destabilize the oxidation state III and thus the $E_{1/2}$ of complex **4** is strongly shifted cathodically by 169 mV ($E_{1/2}=0.006$ V; $E_{p,a}=0.076$ V, $E_{p,c}=-0.063$ V, $\Delta E=139$ mV). On the other hand electron donors in the phenyl ring, as in complex **3**, produce the opposite effect and stabilize Cu^{III} by shifting the $E_{1/2}$ anodically by 38 mV ($E_{1/2}=-0.201$ V; $E_{p,a}=-0.152$ V, $E_{p,c=}-0.250$ V, $\Delta E=98$ mV). Tertiary amines have a lower σ-donating capacity than secondary amines owing to a lower overlap capacity and also solvation effects (*N*-methylation effect) and this is usually manifested in a cathodic shift of the $E_{1/2}$ redox potential. This is observed in complex **5** in which the central secondary amine of the L^2 ligand has been replaced by a methylated tertiary amine and has a significant cathodic shift of 60 mV ($E_{1/2}=-0.103$ V; $E_{p,a}=-0.056$ V, $E_{p,c}=-0.150$ V, $\Delta E=94$ mV). In complex **6** there are two competing electronic effects, the enhanced electron-donating capacity of the methylated phenyl group versus the reduced σ-donating ability of the tertiary amine; overall a 34 mV cathodic shift is observed for complex **6** ($E_{1/2}=-0.129$ V; $E_{p,a}=-0.084$ V, $E_{p,c}=-0.174$ V, $\Delta E=90$ mV).

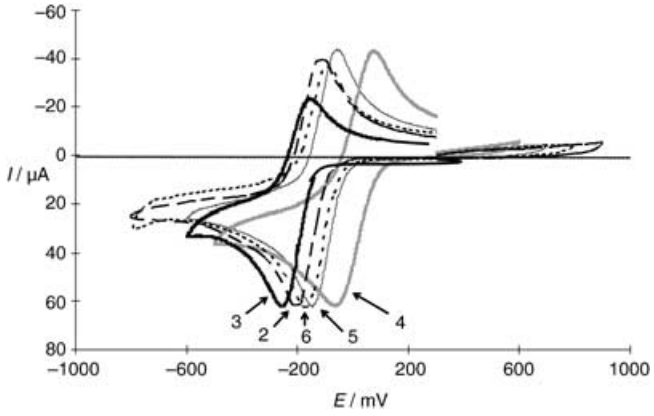

Figure 7. Cyclic voltammograms of complexes **2**–**6** (see text for experimental details).

Furthermore, the electronic effects correlate with the kinetic stability of the corresponding Cu^{II} complexes; thus complex **4** has the largest I ($I_{p,a}/I_{p,c}$), whereas complex **3** has the lowest, showing that electron-withdrawing groups stabilize the Cu^{II} oxidation state whereas electron-donating groups destabilize Cu^{II} and thus the coupled chemical reaction becomes more significant after electron transfer.

The behavior of complex **7** is radically different displaying an irreversible cathodic wave at −0.400 V. The cyclic voltammogram of complex **8** reveals a reversible process in the cyclic voltammetry timescale but it has the largest peak splitting by far ($E_{1/2}=-0.271$ V; $E_{p,a}=-0.148$ V, $E_{p,c}=-0.394$ V, $\Delta E=246$ mV).

Conclusions

A family of Cu complexes in the unusual oxidation state of +3 and containing triazamacrocyclic ligands has been described and their structural, spectroscopic, and redox properties thoroughly investigated. This has allowed us to unravel the detailed electronic structure of these Cu^{III} complexes which in turn permitted us to rationalize their redox and spectroscopic properties. As a result of this detailed work it

has been possible to measure the electronic effects of *N*-methylation in a quantitative manner.

Experimental Section

Materials: All reagents used in this work were obtained from Aldrich Chemical Co. and were used without further purification. Reagent-grade organic solvents were obtained from SDS and high purity deionized water was obtained by passing distilled water through a nanopure Mili-Q water purification system.

Instrumentation and measurements: IR spectra were recorded with a Mattson Satellite FT-IR spectrometer using KBr pellets or by using a MKII Golden Gate Single Reflection ATR System. UV/Vis spectroscopy was performed by using a Cary 50 Scan (Varian) UV/Vis spectrophotometer with 1 cm quartz cells. NMR spectra were recorded with a Bruker 500 MHz or 200 Model Avance spectrometer. Samples were analyzed in either $CDCl_3$ or in [D_3]acetonitrile, with residual solvent protons and/or tetramethylsilane as internal references. Elemental analyses were performed with a CHNS-O Elemental Analyser EA-1108 from Fisons. The ESI-MS experiments were performed on a Navigator LC/MS chromatograph from Thermo Quest Finnigan using methanol or acetonitrile as a mobile phase.

Cyclic voltammetric (CV) experiments were performed in a PAR 263A EG&G or IJ-Cambria IH-660 potentiostat with a three-electrode cell. Glassy carbon disk electrodes (3 mm diameter) from BAS were used as the working electrode, platinum wire as the auxiliary and SSCE as the reference electrode (unless explicitly mentioned in the text, the potentials given are always with respect to this reference electrode). The ferrocene/ferrocenium couple was used as the internal reference with $E_{1/2}$ (versus SSCE) = 371 mV. The complexes were dissolved in previously degassed 0.1 M (nBu$_4$N)(PF_6) in acetonitrile as the supporting electrolyte. All $E_{1/2}$ values reported in this work were estimated from cyclic voltammetry as the average of the oxidative and reductive peak potentials $(E_{p,a}+E_{p,c})/2$ (scan rate = 100 mV s^{-1}, room temperature). The concentration of the complexes was 2 mM. Bulk electrolyses were carried out in a three-compartment cell using carbon felt from SOFACEL as the working electrode.

Sample preparations: **Caution!** Some complexes described in this section contain the perchlorate anion; even though we have not suffered any explosion, perchlorate salts are potentially explosive.

Ligands: All ligands have been prepared following two different methods previously used for the synthesis of HL^1 and HL^2[5,13,14] although HL^2 and HL^5 have previously been prepared following different synthetic routes.[15] The remaining ligands have been synthesized in this work for the first time.

Ligand HL^3: *N*-(3-Aminopropyl)propane-1,3-diamine (3.45 g, 25.7 mmol) was tosylated with TsCl (16.45 g, 85.0 mmol) in THF/H_2O (200 mL) in the presence of NaOH (4.21 g, 103.1 mmol) at 60 °C overnight to give a 52% yield of tritosylated amine (7.95 g, 13.40 mmol) after purification by column chromatography (silica gel, CH_2Cl_2/ethyl acetate 92:8). 3,5-Bis-(bromomethyl)toluene (1.11 g, 4.01 mmol) and the tritosylated amine (2.38 g, 4.01 mmol) in CH_3CN (250 mL) was refluxed for 24 h to give, prior to purification by column chromatography on silica gel (CH_2Cl_2/ethyl acetate 98:2), the desired cyclized tosylated product HL^3 (2.28 g, 3.22 mmol) in 80% yield. Detosylation of tosylated HL^3 was achieved by reduction with lithium in liquid ammonia (approx. 250 mL) at −70 °C. Lithium metal was added until the solution turned deep blue. After 1 hour, NH_4Cl (15 g, 0.28 mol) was added and NH_3 carefully evaporated. Extraction with $CHCl_3$/1 M HCl, evaporation of the aqueous phase, basification with 30% NaOH, extraction with $CHCl_3$, and final purification on silica gel (CH_2Cl_2/MeOH/NH_4OH 80:20:5) yielded ligand HL^3 (0.42 g, 1.71 mmol, 48% yield). ^{1}H NMR (200 MHz, $CDCl_3$, 25 °C): δ = 7.47 (s, 1H; H_x), 6.86 (m, 2H; H_z), 3.84 (s, 4H; H_a), 2.76 (t, J(H,H) = 5.4 Hz, 4H; H_b), 2.53 (t, J(H,H) = 5.8 Hz, 4H; H_d), 2.31 (s, 3H; H_f), 1.69 ppm (quint, J(H,H) = 5.6 Hz, 4H; H_c); ^{13}C NMR (50.3 MHz, $CDCl_3$, 298 K): δ = 141.07, 137.63, 127.65, 121.56 ($C_{aromatic}$), 52.78 (C_a), 46.44 (C_b), 44.01 (C_d), 28.84 (C_c), 21.17 ppm (C_f); ESI-MS (CH_3CN): m/z(%): 248 [HL^3+H]$^+$; elemental analysis calcd (%) for $C_{15}H_{25}N_3$ (247.38): C 72.83, H 10.19, N 16.99; found: C 73.01, H 10.23, N 16.85.

A similar procedure was used to synthesize the rest of the ligands.

Ligand HL^4: Yield: 35%. ^{1}H NMR (200 MHz, $CDCl_3$, 25 °C): δ = 8.20 (s, 1H; H_x), 7.91 (s, 2H; H_z), 3.98 (s, 4H; H_a), 2.79 (t, J(H,H) = 5 Hz, 4H; H_b), 2.56 (t, J(H,H) = 6 Hz, 4H; H_d), 1.70 ppm (quint, J(H,H) = 6 Hz, 4H; H_c); ^{13}C NMR (50.3 MHz, $CDCl_3$, 25 °C): δ = 143.17, 131.41, 121.46 ($C_{aromatic}$), 52.54 (C_a), 46.43 (C_b), 44.49 (C_d), 29.12 ppm (C_c); ESI-MS (CH_3CN): m/z(%): 279 [HL^4+H]$^+$; elemental analysis calcd (%) for $C_{14}H_{22}N_4O_2$ (278.35): C 60.41, H 7.97, N 20.13; found: C 60.85, H 8.24, N 20.50.

Ligand HL^6: Yield: 40%. ^{1}H NMR (200 MHz, $CDCl_3$, 25 °C): δ = 7.39 (s, 1H; H_x), 6.84 (s, 2H; H_z), 3.86 (s, 4H; H_a), 2.57 (t, J(H,H) = 6 Hz, 4H; H_b), 2.42 (t, J(H,H) = 4 Hz, 4H; H_d), 2.30 (s, 3H; H_f), 2.01 (s, 3H; H_e), 1.63 ppm (quint, J(H,H) = 5 Hz 4H; H_c); ^{13}C NMR (50.3 MHz, $CDCl_3$, 25 °C): δ = 140.49, 137.56, 127.01, 121.49 ($C_{aromatic}$), 55.84, 52.64 (CH_2-CH_2-CH_2), 44.92 (C_a), 40.80 (C_e), 27.36 (C_c), 21.16 ppm (C_f); IR (KBr): $\tilde{\nu}$ = 3292 (s), 2916 (s), 2789 (s), 1604 (m), 1459 (s), 1127 (s), 730 cm^{-1} (s); ESI-MS (CH_3CN): m/z(%): 262 [HL^6+H]$^+$; elemental analysis calcd (%) for $C_{16}H_{27}N_3$ (261.41): C 73.51, H 10.41, N 16.07; found: C 73.73, H 10.62, N 15.87.

Synthesis of complexes: The synthesis of complexes [$Cu^{III}(L^1)$](ClO_4)$_2$ (**1**-(ClO_4)$_2$), [$Cu^{III}(L^2)$](ClO_4)$_2$ (**2**-(ClO_4)$_2$), and [$Cu^{III}(L^5)$](ClO_4)$_2$ (**5**-(ClO_4)$_2$) have been reported previously.[5] However, the synthesis of all complexes have been reproduced in this work and in the case of **2**-(ClO_4)$_2$, good crystals for structural resolution were obtained.

[$Cu^{III}(L^3)$](OTf)$_2$, 3-(OTf)$_2$: Equimolar amounts of ligand HL^3 (15.4 mg, 0.062 mmol) and $Cu^{II}(ClO_4)_2$·6H_2O (23.0 mg, 0.062 mmol) were dissolved in CH_3CN (2 mL) under magnetic stirring and under either N_2 or Ar. After 30 min, the resulting orange solution was filtered through celite. Slow diffusion of diethyl ether into the filtered solution over 24 h led to the formation of orange crystals of **3**-(OTf)$_2$ in 50% isolated yield (19.0 mg, 0.031 mmol). ^{1}H NMR (500 MHz, CD_3CN, 25 °C): δ = 6.96 (m, 2H; H_α), 6.78 (s, 2H; H_z), 4.65 (d, ^2J(H,H) = 16 Hz, 2H; H_{a1}), 4.42 (d, ^2J-(H,H) = 16 Hz, 2H; H_{a2}), 3.27 (m, 2H; H_{b1}), 3.15 (m, 2H; H_{b2}), 3.10 (m, 2H; H_{d2}), 2.90 (m, 2H; H_{d1}), 2.31 (s, 3H; H_f), 2.10 (m, 2H; H_{c1}), 1.98 ppm (m, 2H; H_{c2}); IR (KBr): $\tilde{\nu}$ = 3140 (m), 2925 (m), 2857 (m), 1456 (w), 1433 (w), 1279 (s), 1255 (s), 1170 (s), 1029 (s), 636 (m), 517 cm^{-1} (w); UV/Vis (CH_3CN): λ_{max} (ε) = 482 nm (sh, 322 M^{-1}cm^{-1}); ESI-MS (CH_3CN): m/z (%): 458 [**3**-(OTf)]$^+$; elemental analysis calcd (%) for $C_{17}H_{24}N_3CuF_6S_2O_6$ (608.1): C 33.58, H 3.98, N 6.91, S 10.55; found: C 33.75, H 4.06, N 6.67, S 10.44.

The labels used in the NMR assignment for this and all the other complexes are given in Scheme 3.

The same procedure was followed using $Cu^{II}(ClO_4)_2$ as the Cu^{II} salt and the complex was obtained in quantitative yield. Complexes **4** and **6** were synthesized following the same procedure, except for the addition of the appropriate ligand, and yields identical to that of **3** were obtained. Thus only their analytical and spectroscopic data will be given.

[$Cu^{III}(L^4)$](OTf)$_2$, 4-(OTf)$_2$: Yield: 50%. ^{1}H NMR (200 MHz, CD_3CN, 25 °C): δ = 7.9 (s, 2H; H_z), 4.75 (d, ^2J(H,H) = 16 Hz, 2H; H_{a1}), 4.55 (d, ^2J-(H,H) = 16 Hz, 2H; H_{a2}), 3.12 (m, 2H; H_{d1}), 2.97 (m, 2H; H_{d2}), 2.64 (m, 4H; H_{b1}, H_{b2}), 1.96 ppm (m, 4H; H_{c1}, H_{c2}); UV/Vis (CH_3CN): λ_{max} (ε) = 400 nm (sh, 318 M^{-1}cm^{-1}); ESI-MS (CH_3CN): m/z (%): 490 [**4**-(OTf)]$^+$.

[$Cu^{III}(L^6)$](OTf)$_2$, 6-(OTf)$_2$: Yield: 50% (18.3 mg, 0.029 mmol) ^{1}H NMR (500 MHz, CD_3CN, 25 °C): δ = 7.71 (m, 2H; H_α), 6.77 (s, 2H; H_z), 4.67 (d, ^2J(H,H) = 16 Hz, 2H; H_{a1}), 4.52 (d, ^2J(H,H) = 16 Hz, 2H; H_{a2}), 3.37 (m, 2H; H_{b1}), 3.21 (m, 2H; H_{d1}), 3.15 (dt ,^3J(H,H) = 3.3 Hz, ^2J(H,H) = 13.3 Hz, 2H; H_{b2}), 2.91 (s, 3H; H_e), 2.68 (m, 2H; H_{d2}), 2.33 (m, 2H; H_{c1}), 2.28 (s, 3H; H_f), 2.02 ppm (m, 2H; H_{c2}); IR (KBr): $\tilde{\nu}$ = 3139 (m), 2925 (m), 2857 (m), 1452 (w), 1435 (w), 1279 (s), 1259 (s), 1170 (s), 1031 (s), 636 (m), 518 cm^{-1} (w); UV/Vis (CH_3CN): λ_{max} (ε) = 496 nm (sh, 218 M^{-1}cm^{-1}); ESI-MS (CH_3CN): m/z(%): 472 [**6**(OTf)]$^+$; elemental analysis calcd (%) for $C_{17}H_{24}N_3CuF_6S_2O_6$ (608.1): C 34.75, H 4.21, N 6.75, S 10.31; found: C 34.53, H 4.32, N 6.67, S 10.32.

[$Cu^{III}(L^2)$(Cl)](OTf), 7-(OTf): Complex **2**-(OTf)$_2$ (0.022 g, 0.037 mmol) was dissolved in CH_3CN (2 mL) and NaCl (1 equiv, 0.0022 g) in H_2O

(0.5 mL) was added. After the addition of NaCl the original orange solution turned red immediately. The solution was then magnetically stirred for 30 min and filtered. Diffusion of diethyl ether into the filtrate led to the formation of red crystals of **7**(OTf) in 73% isolated yield (0.012 g, 0.026 mmol). ^{1}H NMR (400 MHz, CD_3CN, 25°C): $\delta = 7.12$ (t, $^3J(H,H) = 7.5$ Hz, 1H), 6.81 (d, $^3J(H,H) = 3.6$ Hz, 2H)), 6.07 (m, 2H; NH), 4.38 (m,2H), 4.25 (m, 2H), 3.14 (m, 3H), 2.80 (m, 6H), 1.89 (m, 1H), 1.70 ppm (m, 2H); IR (KBr): $\tilde{\nu} = 3126$, 3090, 3033, 2926, 2854, 1459, 1423, 1144, 1116, 1078, 627 cm^{-1}; UV/Vis (CH_3CN): λ_{max} (ε) = 375 (1900), 522 nm (540 $M^{-1}cm^{-1}$). Crystals of $[Cu^{III}(L^2)(Cl)](ClO_4)$, **7**-($ClO_4$), suitable for X-ray diffraction were synthesized by the same procedure.

$[Cu^{III}(L^4)(Cl)](OTf)$, 8-(OTf): This complex was prepared in solution only. UV/Vis (CH_3CN): λ_{max} (ε) = 365 nm (2900 $M^{-1}cm^{-1}$), 503 nm (308 $M^{-1}cm^{-1}$)

X-ray structure determination: The structures of **1**-$(ClO_4)_2$ and **5**-$(ClO_4)_2$ have been published previously.[5]

An orange crystal of **2**-$(OTf)_2$, a red crystal of **6**-$(OTf)_2$, and a parallepiped dark-red crystal of **7**-(ClO_4) were placed on a STOE imaging plate diffraction system (I.P.D.S) equipped with an Oxford Cryosystems Cryostream Cooler Device. These crystals were studied by X-ray diffraction using graphite-monochromated $Mo_{K\alpha}$ radiation ($\lambda = 0.71073$ Å) operating in the ϕ scan method. The cell measurement temperature was 180(2) K for **1**-$(ClO_4)_2$ and **6**-$(OTf)_2$, and 160(2) K for **2**-$(OTf)_2$ and **7**-(ClO_4). Their structures were solved by direct methods using the SIR92 program,[23] and subsequent difference Fourier maps. The models were refined by least-squares procedures on F^2 with the aid of SHELX-97.[24]

Statistical disorder was found on the atoms labeled N2 and C5 in complex **1** and is located on the two sites with a ratio of occupancy close to 50%. Disorder was also found on the SO_3 group of the triflate anion in complex **6**-$(OTf)_2$ and was found to be statistically distributed between the two sites in a ratio of occupancy equal to 50%; some restraints were introduced on interatomic distances and angles in order to regularize the geometry of the SO_3 group. Further, disordered perchlorate oxygen atoms were also found in complex **7**-(ClO_4), which contains two almost identical molecules of the chloro cationic complex.

Data reduction, Lorentz polarization, and empirical absorption corrections were performed using the Sadabs package. Structures were solved by direct methods using SHELXS-86,[25] and refined by full-matrix least-squares analyses with SHELXL-93.[26]

CCDC-261432 (**2**), CCDC-261433 (**3**), CCDC-261434 (**6**), and CCDC-261435 (**7**) contain the supplementary crystallographic data for this paper. These data can be obtained free of charge from the Cambridge Crystallographic Data Centre via www.ccdc.cam.ac.uk/data_request/cif.

Computational details: The reported calculations were carried out by using the Amsterdam density functional (ADF) package developed by Baerends and co-workers[27–29] and vectorized by Ravenek.[30] The numerical integration scheme employed was that of te Velde and Baerends.[31]

Both geometry optimizations and energy evaluations were performed using a generalized gradient approximation (GGA) that includes Becke's GGA exchange correction[32] and Perdew's GGA correlation correction.[33] Experimentally it was found that these mononuclear species are diamagnetic. For this reason, optimizations were carried out for neutral closed-shell singlet ground-state structures. However, we have checked the relative stabilities of the singlet and triplet states of all the calculated complexes. In all cases, the triplet state has a higher energy. This is in agreement with the sharp peaks in the diamagnetic regions of the NMR spectra. The difference between the two states is around 25 kcal mol^{-1} in all the cases studied.

The UV spectra were simulated by the time-Dependent DFT method (TDDFT),[34] using the LB94 potential of van Leeuwen and Baerends.[35]

The 2000.02 release of the ADF package was used for all geometry optimizations and the calculated UV/Vis spectra were obtained by using the 2002.03 release of the ADF program.[36]

In the geometry optimizations we used an uncontracted triple-ς basis set to describe the 3s, 3p, 3d, 4s, and 4p orbitals of copper. For carbon (2s,2p), nitrogen (2s,2p), oxygen (2s,2p), and hydrogen (1s), double-ς basis sets were employed and augmented by an extra polarization function.[37,38] Electrons in lower shells were treated within the frozen-core approximation.[27] A set of auxiliary s, p, d, f, and g functions, centered in all nuclei, was introduced in order to fit the molecular density and Coulomb potential accurately in each SCF cycle.[39] For the particular case of **2**, the experimental and theoretical bond lengths and angles differ by less than 0.07 Å and 3.0°, respectively. The standard deviation for the bond distances is 0.03 Å, and for the angles 1.81°. The standard deviation is calculated using Equation (2), where CV means calculated value, EV experimental value (X-ray data), and N is the number of bond distances or angles taken into account. See the Supporting Information for the bond distances and angles used to calculate s_{n-1}.

$$s_{n-1} = \sqrt{\frac{\sum_{i=1}^{N} (\mathrm{CV}-\mathrm{EV})^2}{N-1}} \qquad (2)$$

To simulate the UV/Vis spectra an uncontracted triple-ς basis set was used for all the atoms. For the copper atom this basis set was augmented by an extra polarization function.[37,38] We have checked in several complexes that the inclusion of diffuse functions in the basis set and relativistic effects in the hamiltonian only produce slight changes in the positions of the bands, and therefore to reduce the computational cost these effects have not been taken into account.[40]

The effect of solvent on the UV/Vis spectra was considered by using the conductor-like screening model (COSMO) of Klamt and Schüürmann,[41] as implemented by Pie and Ziegler in the ADF program.[42] The radius chosen for the solvent [2.75 Å for acetonitrile ($\varepsilon = 37.50$)][43] was obtained by calculating the molecular volume with the Gaussian 98 package.[44] The radii used for the C, N, Cl, H, O, and Cu atoms were 2.00, 1.40, 1.20, 1.18, 1.30, and 1.50 Å, respectively.[42]

All molecular orbitals were constructed by using the MOLEKEL program.[45]

Acknowledgements

This research has been financed by the MCYT of Spain through projects BQU2003-02884, BQU2003-01677 and BQU2002-04112-C02-02. A.L. and M.S. are grateful to the CIRIT Generalitat de Catalunya (Spain) for the Distinction award and A.L. is grateful for aid through SGR2001-UG-291. A.L. also thanks Johnson and Matthey for the loan of platinum metal. X.R. is grateful for a Juan de la Cierva contract from the MEC. R.X. and A.P. are grateful for the award of doctoral grants from the UdG and the MEC, respectively.

[1] a) J. P. Collman, L. S. Hegedus, J. R. Norton, R. G. Finke in *Principles and Applications of Organotransition Metal Chemistry*, 2nd ed., University Science, Mill Valley, **1987**, Chapter 7; b) A. E. Martell, D. T. Sawyer, *Oxygen Complexes and Oxygen Activation by Transition Metals*, Texas A & M University, **1987**; c) M. D. Fryzuk, S. A. Johnson, *Coord. Chem. Rev.* **2000**, *200–202*, 379–409; d) M. Albrecht, G. van Koten, *Angew. Chem.* **2001**, *113*, 3866–3898; *Angew. Chem. Int. Ed.* **2001**, *40*, 3750–3781; e) W. D. Jones, *Acc. Chem. Res.* **2003**, *36*, 140–146; f) M. E. van der Boom, D. Milstein, *Chem. Rev.* **2003**, *103*, 1759–1792.

[2] a) J. A. Labinger, J. E. Bercaw, *Nature* **2002**, *417*, 507–514; b) J. M. Thomas, R. Raja, G. Sankar, R. G. Bell, *Acc. Chem. Res.* **2001**, *34*, 191–200; c) H. Chen, S. Schlecht, T. C. Semple, J. F. Hartwig, *Science* **2000**, *287*, 1995–1997; d) R. H. Crabtree, *Chem. Rev.* **1995**, *95*, 987–1007; e) A. E. Shilov, G. B. Shul'pin, *Chem. Rev.* **1997**, *97*, 2879–2932.

[3] M. J. Gradassi, N. W. Green, *Fuel Process. Technol.* **1995**, *42*, 65–83.

[4] M. Gandelman, L. J. W. Shimon, D. Milstein, *Chem. Eur. J.* **2003**, *9*, 4295–4300.

[5] X. Ribas, D. A. Jackson, B. Donnadieu, J. Mahía, T. Parella, R. Xifra, B. Hedman, K. O. Hodgson, A. Llobet, T. D. P. Stack, *Angew. Chem.* **2001**, *113*, 3117–3120; *Angew. Chem. Int. Ed.* **2002**, *41*, 2991–2994.
[6] L. L. Diaddario, W. R. Robinson, D. L. Margerum, *Inorg. Chem.* **1983**, *22*, 1021–1025.
[7] I. H. Wasbotten, T. Wondimageng, A. Ghosh, *J. Am. Chem. Soc.* **2002**, *124*, 8104–8116.
[8] a) H. Furuta, H. Maeda, A. Osuka, *J. Am. Chem. Soc.* **2000**, *122*, 803–807; b) M. Stepien, L. Latos-Grazynski, *Chem. Eur. J.* **2001**, *7*, 5113–5117.
[9] a) M. A. Willert-Porada, D. J. Burton, N. C. Baenziger, *J. Chem. Soc., Chem. Commun.* **1989**, 1633–1634; b) D. Naumann, T. Roy, K. F. Tebbe, W. Crump, *Angew. Chem.* **1993**, *105*, 1555–1556; *Angew. Chem. Int. Ed. Engl.* **1993**, *32*, 1482–1483; c) R. Eujen, B. Hoge, D. J. Brauer, *J. Organomet. Chem.* **1996**, *519*, 7–20.
[10] a) T. D. P. Stack, *Dalton Trans.* **2003**, 1881–1889; b) N. W. Aboelella, E. A. Lewis, A. M. Reynolds, W. W. Brennessel, C. J. Cramer, W. B. Tolman, *J. Am. Chem. Soc.* **2002**, *124*, 10660–10661.
[11] S. K. Burke, Y. Xu, D. W. Margerum, *Inorg. Chem.* **2003**, *42*, 5807–5817.
[12] D. H. R. Barton, N. C. Delanghe, H. Patin, *Tetrahedron* **1997**, *53*, 16017–16028.
[13] A. Bencini, M. I. Burguete, E. Garcia-España, S. V. Luis, J. F. Miravet, C. Soriano, *J. Org. Chem.* **1993**, *58*, 4749–4753.
[14] C. Bazzicalupi, A. Bencini, A. Bianchi, V. Fusi, E. Garcia-España, P. Paoletti, P. Paoli, B. Valtancoli, *Inorg. Chem.* **1993**, *32*, 4900–4908.
[15] a) K. Hiraki, J. Tsutsumida, Y. Fuchita, *Chem. Lett.* **1986**, 337–340; b) K. Hiraki, Y. Fuchita, Y. Ohta, J. Tsutsumida, K. I. Hardcastle, *J. Chem. Soc., Dalton Trans.* **1992**, 833–836; c) A. Chellini, G. B. Giovenzana, R. Pagliarin, G. Palmisano, M. Sisti, *Helv. Chim. Acta* **2000**, *83*, 793–800.
[16] a) G. Golub, H. Cohen, P. Paoletti, A. Bencini, L. Messori, I. Bertini, D. Meyerstein, *J. Am. Chem. Soc.* **1995**, *117*, 8353–8361; b) D. Meyerstein, *Coord. Chem. Rev.* **1999**, *185–186*, 141–147.
[17] a) P. V. Bernhardt, *J. Am. Chem. Soc.* **1997**, *119*, 771–774; b) P. V. Bernhardt, *Inorg. Chem.* **2001**, *40*, 1086–1092; c) P. V. Bernhardt, P. Comba, T. W. Hambley, *Inorg. Chem.* **1993**, *32*, 2804–2809; d) M. M. Bernardo, M. J. Heeg, R. R. Schroeder, L. A. Ochrymowycz, D. B. Rorabacher, *Inorg. Chem.* **1992**, *31*, 191–198.
[18] It is important to bear in mind the existence of a certain controversy on the purity of the compounds reported in the work published by Meyerstein (see ref. [16a]) and Bernhardt (see ref. [17a]).
[19] a) J. Hanss, H.-J. Krüger, *Angew. Chem.* **1996**, *108*, 2989–2991; *Angew. Chem. Int. Ed. Engl.* **1996**, *35*, 2827–2830; b) J. Hanss, A. Beckmann, H.-J. Krüger, *Eur. J. Inorg. Chem.* **1999**, 163–172.
[20] E. I. Solomon M. E. Hanson in *Inorganic Electronic Structure and Spectroscopy*, *Vol. 2* (Eds.: E. I Solomon, A. B. P. Lever), Wiley, **1999**, Chapter 1.
[21] a) L. Bernasconi, J. Blumberger, M. Sprik, R. Vuilleumier, *J. Chem. Phys.* **2004**, *121*, 11885–11899; b) X. Ribas, J. C. Dias, J. Morgado, K. Wurst, E. Molins, E. Ruiz, M. Almeida, J. Veciana, C. Rovira, *Chem. Eur. J.* **2004**, *10*, 1691–1704; c) Y. Yamaguchi, S. Yokoyama, S. Mashiko, *J. Chem. Phys.* **2002**, *116*, 6541–6548; d) Z.-L. Cai, K. Sendt, J. R. Reimers, *J. Chem. Phys.* **2002**, *117*, 5543–5549.
[22] S. J. A. van Gisbergen, A. Rosa, G. Ricciardi, E. J. Baerends, *J. Chem. Phys.* **1999**, *111*, 2499–2506.
[23] A. Altomare, G. Cascarano, G. Giacovazzo, A. Guagliardi, M. C. Burla, G. Polidori, M. Camalli, *J. Appl. Crystallogr.* **1994**, *27*, 435–436.
[24] SHELX-97 (includes SHELXS97, SHELXL97, CIFTAB), Programs for Crystal Structure Analysis (Release 97–2), G. M. Sheldrick, University of Göttingen (Germany), **1998**.
[25] SHELXS-86, Programs for the Solution of Crystal Structures; G. M. Sheldrick, University of Göttingen (Germany), **1998**.
[26] SHELX-93, G. M. Sheldrick, University of Göttingen (Germany), **1998**.
[27] E. J. Baerends, D. E. Ellis, P. Ros, *Chem. Phys.* **1973**, *2*, 41–51.
[28] C. Fonseca Guerra, O. Visser, J. G. Snijders, G. te Velde, E. J. Baerends, *Methods and Techniques for Computational Chemistry*, STEF, Cagliari, **1995**, p. 305.
[29] G. te Velde, F. M. Bickelhaupt, E. J. Baerends, C. Fonseca Guerra, S. J. A. Van Gisbergen, G. J. Snijders, T. Ziegler, *J. Comput. Chem.* **2001**, *22*, 931–967.
[30] W. Ravenek, *Algorithms and Applications on Vector and Parallel Computers*, Elsevier, Amsterdam, **1987**.
[31] G. te Velde, E. J. Baerends, *J. Comp. Phys.* **1992**, *99*, 84–98.
[32] A. D. Becke, *Phys. Rev. A* **1988**, *38*, 3098–3100.
[33] J. P. Perdew, *Phys. Rev. B* **1986**, *33*, 8822–8824.
[34] a) E. K. U. Gross, J. F. Dobson, M. Petersilka, *Density Functional Theory* (Ed.: R. F. Nalewajski), Springer, Heidelberg, **1996**; b) S. J. A. van Gisbergen, J. G. Snijders, E. J. Baerends, *Comput. Phys. Commun.* **1999**, *118*, 119–138.
[35] R. van Leeuwen, E. J. Baerends, *Phys. Rev. A* **1994**, *49*, 2421–2431.
[36] ADF2002.03, E. J. Baerends, J. A. Autschbach, A. Bérces, C. Bo, P. M. Boerrigter, L. Cavallo, D. P. Chong, L. Deng, R. M. Dickson, D. E. Ellis, L. Fan, T. H. Fischer, C. Fonseca Guerra, S. J. A. van Gisbergen, J. A. Groeneveld, O. V. Gritsenko, M. Grüning, F. E. Harris, P. van den Hoek, H. Jacobsen, G. van Kessel, F. Kootstra, E. van Lenthe, V. P. Osinga, S. Patchkovskii, P. H. T. Philipsen, D. Post, C. C. Pye, W. Ravenek, P. Ros, P. R. T. Schipper, G. Schreckenbach, J. G. Snijders, M. Solà, M. Swart, D. Swerhone, G. te Velde, P. Vernooijs, L. Versluis, O. Visser, E. van Wezenbeek, G. Wiesenekker, S. K. Wolff, T. K. Woo, T. Ziegler, Vrije Universiteit Amsterdam, Amsterdam, **2002**.
[37] G. J. Snijders, E. J. Baerends, P. Vernooijs, *At. Nucl. Data Tables* **1982**, *26*, 483–509.
[38] P. Vernooijs, E. J. Baerends, *Slater Type Basis Functions for the Whole Periodic System. Internal Report*, Vrije Universiteit of Amsterdam, Amsterdam, **1981**.
[39] J. Krijn, E. J. Baerends, *Fit Functions in the HFS Method. Internal Report (in Dutch)*, Vrije Universiteit of Amsterdam, Amsterdam, **1984**.
[40] E. van Lenthe, E. J. Baerends, *J. Comput. Chem.* **2003**, *24*, 1142–1156.
[41] A. Klamt, G. Schüürmann, *J. Chem. Soc., Perkin Trans. 2* **1993**, 799–805.
[42] C. C. Pye, T. Ziegler, *Theor. Chem. Acc.*, **1999**, 101, 396–408.
[43] *Handbook of Chemistry and Physics*, 83rd ed. (Ed.: D. R. Lide), CRC Press, Boca Raton FL, **2002–2003**.
[44] Gaussian 98 (Revision A.11), M. J. Frisch, G. W. Trucks, H. B. Schlegel, G. E. Scuseria, M. A. Robb, J. R. Cheeseman, V. G. Zakrzewski, J. A. Montgomery, Jr., R. E. Stratmann, J. C. Burant, S. Dapprich, J. M. Millam, A. D. Daniels, K. N. Kudin, M. C. Strain, O. Farkas, J. Tomasi, V. Barone, M. Cossi, R. Cammi, B. Mennucci, C. Pomelli, C. Adamo, S. Clifford, J. Ochterski, G. A. Petersson, P. Y. Ayala, Q. Cui, K. Morokuma, P. Salvador, J. J. Dannenberg, D. K. Malick, A. D. Rabuck, K. Raghavachari, J. B. Foresman, J. Cioslowski, J. V. Ortiz, A. G. Baboul, B. B. Stefanov, G. Liu, A. Liashenko, P. Piskorz, I. Komaromi, R. Gomperts, R. L. Martin, D. J. Fox, T. Keith, M. A. Al-Laham, C. Y. Peng, A. Nanayakkara, M. Challacombe, P. M. W. Gill, B. Johnson, W. Chen, M. W. Wong, J. L. Andres, C. Gonzalez, M. Head-Gordon, E. S. Replogle, J. A. Pople, Gaussian, Inc., Pittsburgh PA, **2001**.
[45] MOLEKEL 4.0, P. Flükiger, H. P. Lüthi, S. Portmann, J. Weber, Swiss Center for Scientific Computing, Manno (Switzerland), **2000**.

Received: January 25, 2005
Published online: June 30, 2005